Water **2014**, *6*, 517-546; doi:10.3390/w6030517

OPEN ACCESS

water

ISSN 2073-4441

www.mdpi.com/journal/water

Article

Integrated River and Coastal Hydrodynamic Flood Risk Mapping of the LaHave River Estuary and Town of Bridgewater, Nova Scotia, Canada

Tim Webster *, Kevin McGuigan, Kate Collins and Candace MacDonald

Applied Geomatics Research Group, Nova Scotia Community College, Middleton, Nova Scotia B0S 1M0, NS, Canada; E-Mails: kevin.mcguigan@nscc.ca (K.M.); kate.collins@nscc.ca (K.C.); candace.macdonald@nscc.ca (C.M.)

* Author to whom correspondence should be addressed; E-Mail: timothy.webster@nscc.ca; Tel.: +1-902-825-2775; Fax: +1-902-825-5479.

Received: 12 December 2013; in revised form: 27 February 2014 / Accepted: 5 March 2014 / Published: 21 March 2014

Abstract: Bridgewater, Nova Scotia, is located 20 km inland from the mouth of the LaHave River estuary on the Atlantic Coast of Canada. Bridgewater is at risk of flooding due to the combined effects of river runoff and a storm surge on top of high tide. Projected increases in sea-level and possible increased river runoff with climate change increase the risk of future flooding. A set of river and ocean water level simulations were carried out to determine the risk of flooding to Bridgewater today and in the future under climate change. The hydrodynamic simulation developed incorporates return periods of a time series of river discharge measurements for the LaHave watershed, ocean water dynamics at the mouth of the river under normal tidal conditions and with two levels of storm surge, near shore and river bathymetry, as well as high precision topographic lidar derived ground elevations and survey grade GPS. The study was supported by data from two tide gauge sensors, and qualitative evidence provided by the community such as historical flood levels and photographs. Results show that areas upstream of the town are vulnerable to large discharge events of the LaHave River. The downtown waterfront and infrastructure are not susceptible to fluvial flooding, but is vulnerable to sea-level rise and storm surge flooding.

Keywords: flood risk; hydrodynamic modelling; storm surge; lidar; coupled fluvial-tidal model; sea-level rise; return periods

---

1. Introduction

The Town of Bridgewater, Nova Scotia, Canada is located along the banks of the LaHave River, about 20 km from where the river meets the Atlantic Ocean. Like many coastal communities, Bridgewater is vulnerable to flooding from storm surge and sea-level rise. In addition, high river discharge resulting from heavy rainfall and spring melt water can cause the LaHave River to flood, potentially putting Bridgewater and the surrounding communities at additional risk.

This study has been conducted for the Town of Bridgewater to determine the risk of flooding from LaHave River runoff and from storm surge. Similar studies of flood risk for communities located along major estuaries have been conducted by the Applied Geomatics Research Group as part of the Atlantic Climate Change Adaptation Solutions (ACAS) project [1–4]. Like the previous studies, the flood risk analysis of the LaHave River incorporates high-resolution lidar elevation data, bathymetric river data, and river cross-section information. These data are merged to generate a seamless digital elevation model (DEM) which is used, along with river discharge and tidal elevation data to run an integrated one and two-dimensional hydrodynamic model to produce flood risk predictions for the Town of Bridgewater.

High resolution lidar is an optimal choice for fluvial flood inundation models of urban areas, where capturing the complexities of urban topography is critical to model outcome [5–8]. Lidar-based models of coastal vulnerability to storm surge flooding also depend on the resolution of the DEM [9,10]. A combination of high-resolution lidar-derived DEMs, and historical high water level data have been used to successfully model benchmark coastal storms in Atlantic Canada [11–13] and elsewhere [14].

Bathymetric information is critical to the running of the river and coastal models, and can be acquired through various means. Cin *et al.* [15] combined swath bathymetry and lidar to create a DEM to forecast river flooding, and Moore [16] combined channel geometry acquired from river bathymetric surveys with lidar to generate a high resolution DEM. Higher quality and resolution bathymetry data can improve model results [17,18]. Casas *et al.* [17] investigated the dependence of hydraulic model outcome on digital elevation inputs and show the importance of high quality bathymetric data. Cook and Merwade [18] predicted flood inundation area more accurately with improved horizontal resolution, vertical accuracy, and the inclusion of river bathymetry in the topographic data. Though high resolution topo-bathymetic data is advantageous for developing accurate hydrodynamic shallow water and flooding simulations, it is important to minimize data density where possible to reduce the CPU time required for the complex calculations. As such, in this study we model the lower mouth of the estuary in a coarser grid resolution and nest higher resolution simulations for the upstream town area, where a higher resolution flood simulation output is desired.

For this study a bathymetric survey was conducted using a depth sounder and Real Time Kinematic (RTK) GPS to acquire data for the upper sections of the LaHave estuary, and RTK GPS cross-sections in the shallower areas of the river. The final DEM used for the river and coastal flooding models includes high-resolution lidar on land, bathymetric data for the river channel and coast acquired during this study, and a combination of digital and digitized paper charts for the outer estuary where available. We present a unique method to combine the bathymetry and river cross section data with the lidar to construct a seamless DEM, which is then used to approximate cross sections for the 1-D upstream model in areas where cross sections do not exist, and perform seamless 2-D shallow water and flood modelling without complex 1-D/2-D shore linkages and weir flow calculations.

A coupled 1-D/2-D model is used here to take advantage of the benefits of each model. The 1-D model is best used to represent hydraulic flow through the channel, while the 2-D model is required for spatially distributed results, such as flood inundation maps [19]. Previous coupled 1-D/2-D modeling studies of coastal flooding focus on the failure of sea defense mechanisms [20,21], and Brown *et al.* [20] and Webster *et al.* [22] note the significance of forcing inputs, such as coastal water levels, to model outcome, and cite the ongoing issue of model sensitivity to spatial resolution of the grid. In this study, we have not focused on variations in grid density for the large domain, but rather in selected areas with the goal of achieving our desired flood inundation mapping precision for the town while keeping the CPU calculation time reasonable for each simulation.

We analyzed a time series of river discharge records to derive an extreme value model for the LaHave River to calculate the discharge for the 50 and 100 year return periods at probabilities of occurrence of 65 and 99.5 percent which represents the upstream boundary condition in our 1D model. This was coupled with a 2-D coastal model of mean high tide conditions and two elevated sea-levels representing storm surge and sea-level rise in the future.

We employ the Danish Hydraulic Institute (DHI) coupled 1-D/2-D Mike Flood™ model which integrates a one-dimensional numerical model of the river channel with a two-dimensional model of the floodplain. This model is a common choice for flood prediction mapping using lidar-based DEMs [23,24]. Gilles *et al.* [23] modeled fluvial flood events in Iowa successfully by calibrating the model to measured water levels in the river and floodplain. Patro *et al.* [24] modeled monsoon flooding on an Indian river delta and found the model to be quite satisfactory in simulating river flow and flood inundation extent. Sto. Domingo *et al.* [25] used Mike Flood ^{TM} to do an analysis of flooding from sea-level rise and storm surges in major cities under climate change scenarios; and found the coupled model to be better than "Terrain Analysis" approaches at mapping flooding from the sea.

1.1. Study Area

The LaHave River watershed covers 1686 km^2, extending from Riverport at the coast to the south side of South Mountain in the Annapolis Valley (Figure 1). The watershed contains a mix of land use, including industrial and residential within the Town of Bridgewater, and shifting to mainly forested and agricultural in the majority of the watershed.

The LaHave watershed includes two Ecodistricts, as defined by the Nova Scotia Department of Natural Resources [26]. The LaHave Drumlins Ecodistrict is characterized by glacial till drumlins and coniferous forests, with soils that are mostly well-drained, except between the drumlins where soil is poorly drained. The LaHave River flows through the center of the Ecodistrict until it enters the South Shore Ecodistrict near the coast. The South Shore Ecodistrict is composed of a mixture of sandy beaches, lakes and streams, and coastal forests.

Tides are semi-diurnal in the Bridgewater area, with a tidal range of 2.5 m. The tidal influence extends ~20 km up the LaHave River, just to downtown Bridgewater. The river does not ice over during the winter, but ice does form upstream of the town and in the lakes and throughout the watershed.

1.2. Coastal Flooding

The Canadian Hurricane Center (CHC) states that one or two tropical cyclone events (hurricanes or tropical storms) affect Canada per year [27], and the beaches near Bridgewater are regularly battered by Nor'easters, tropical storms and occasionally a hurricane. Powerful wind, waves, and storm surges can cause damage to dunes and beach infrastructure, coastal properties and roadways. Hurricane Hortense (1996), Hurricane Juan (2003), post-tropical storm Noel (2007), and Hurricane Bill (2009) caused significant damage to the coast near Bridgewater [28,29]. Bridgewater enjoys some protection from coastal storm surge because it is nearly 20 km inland and because of a sharp bend in the LaHave River near the coast (Figure 1). However, it is not immune to storm surge-induced flooding. A low pressure system brought high winds and heavy rain to the area on 30 October 2011, causing a storm surge that flooded some areas of downtown Bridgewater. Unfortunately, there is no tidal record for the LaHave River; therefore no storm surge return period analysis has been completed for the Town of Bridgewater directly. A 1 m storm surge was measured at the Halifax tide gauge, the closest gauge to Bridgewater, during this event located 60 km northeast along the Atlantic Coast (Figure 1).

Figure 1. The Town of Bridgewater is an inland coastal community located along the banks of the LaHave River in the southern region of Nova Scotia, Canada. A: AGRG Cherryfield weather station; B: Environment Canada water level gauge; C: AGRG Marine Terminal tide gauge; D: AGRG Kraut Point tide gauge; E: AGRG Hirtles Beach weather station.

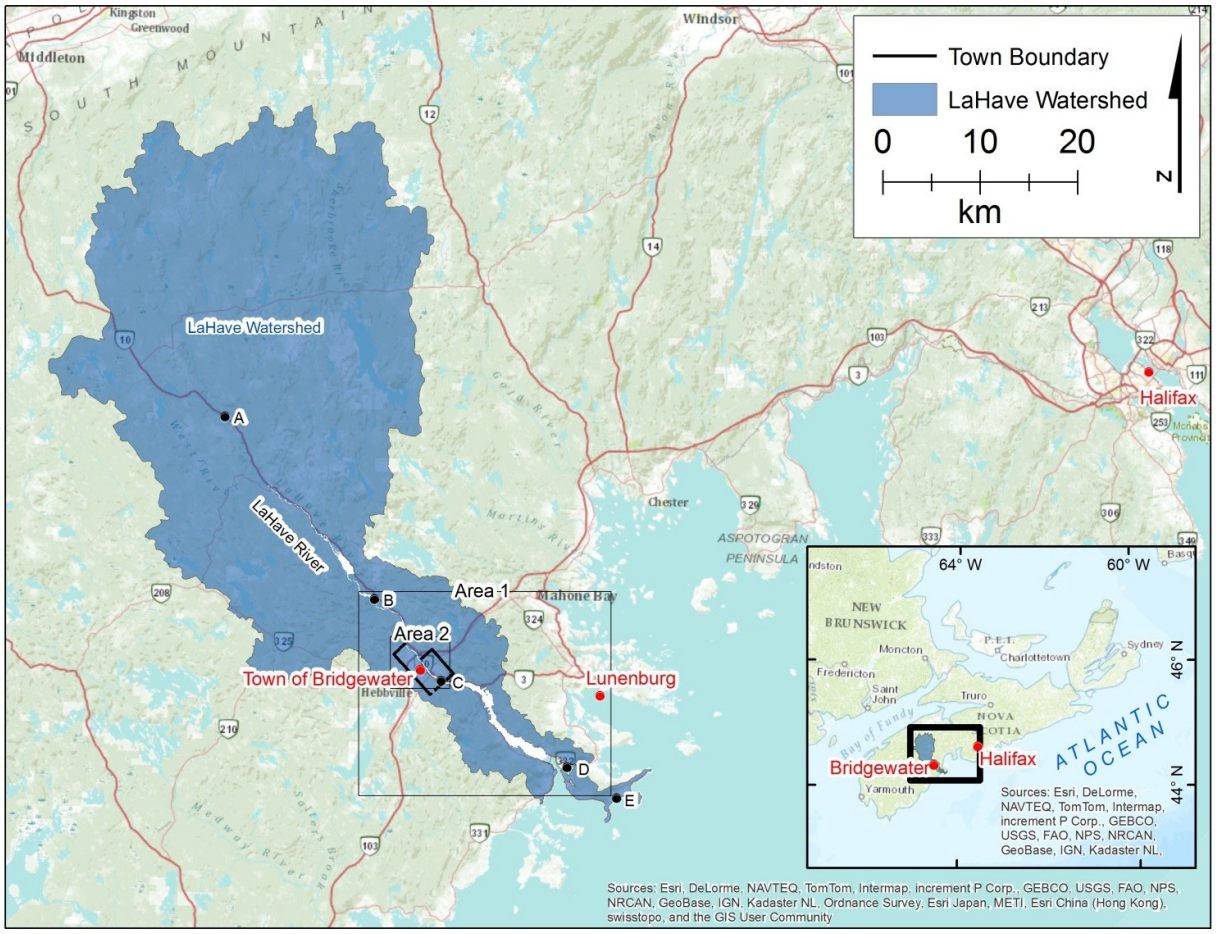

1.3. Sea-Level Rise and Climate Change

The global climate is changing due in part to the increase of greenhouse gas emissions, and the resulting warming trends will contribute to an increase of global sea-level [30]. Future projections of sea-level change depend on estimated future greenhouse gas emissions and are predicted based on a number of scenarios [31]. Global sea-level rise, as predicted by climate change models, will increase the problem of flooding and erosion making more coastal areas vulnerable. The third assessment of the Intergovernmental Panel on Climate Change (IPCC), AR3, indicated that there will be an increase in mean global sea-level from 1990 to 2100 between 0.09 m and 0.88 m [32]. The fourth IPCC Assessment Report (AR4) projected global mean sea-level to rise between 0.18 and 0.59 m from 1990 to 2095 [33]. However as Forbes *et al.* [34] point out, these projections do not account for the large ice sheets melting and measurements of actual global sea-level rise are higher than the previous predictions of the third assessment report. The most recent IPCC estimates for global sea-level rise were available in a preliminary document, the Summary for Policymakers [30], at the time of submission. The authors project a sea-level rise for 2046–2065 of 0.17 m to 0.38 m (lower bound higher than AR3 and ~same as AR4) and for 2081–2100 of 0.26 m to 0.82 m (upper bound slightly lower than AR3, 0.23 m higher than AR4); these projections do include the effects of melting ice sheets.

Rahmstorf *et al.* [35] compared observed global sea-level rise to that projected in the third IPCC assessment report and found it exceeded the projections. They have suggested a rise between 0.5 and 1.4 m from 1990 to 2100. This projected increase in global mean sea-level and the fact that many coastal areas of Maritime Canada have been deemed highly susceptible to sea-level rise [36] has led to various studies to produce detailed flood risk maps of coastal communities in Prince Edward Island, New Brunswick, and Nova Scotia [9,37–39]. The most recent set of flood risk maps for coastal communities in Nova Scotia has been produced during the Atlantic Climate Adaptation Solutions (ACAS) project [2,4].

In addition to global sea-level rise, local crustal dynamics also affect relative sea-level (RSL). The major influence on crustal motion for this region is related to the last glaciation that ended *ca*. 10,000 years ago [40–42]. The areas where the ice was thickest were depressed the most and peripheral regions where uplifted, termed the "peripheral bulge". The ice was thickest over Hudson Bay in central Canada, where the crust was most depressed, however today this area is still rebounding from the removal of the ice load and continues to uplift. The Maritimes represent part of the peripheral bulge and southern New Brunswick and Nova Scotia are subsiding [42]. Subsidence rates vary across the region with Nova Scotia having a rate of ~15 cm per century [34]. The subsidence of the crust is important for coastal communities in that it compounds the problem of local sea-level rise and must be considered when projecting future flood risk. Global sea-level rise and crustal subsidence must both be considered to produce a potential increase in RSL in the next century. This does not include the possibility of increased storm intensity or frequency. Although the CHC states that hurricane frequency follows a 25-year cyclical pattern, and we are now in a more active cycle, others claim that hurricane frequency and intensity are increasing with climate change [43,44].

We have selected a conservative and a higher rate of global sea-level rise to illustrate the impacts of past storms into the future. We use global mean sea-level projections from the third IPCC assessment [33] (AR4, A1F1 scenario) as the conservative rate (0.57 m); the higher rate (1.3 m) comes from

Rahmstorf [35]. Assuming a crustal subsidence rate of 0.16 m [34] the upper limit of relative sea-level rise projections for 2100 are 0.57 m + 0.16 m = 0.73 m [33] and 1.3 m + 0.16 m = 1.46 m [35].

A comprehensive, community-by-community report prepared for ACAS by Richards and Daigle [45] provides estimated extreme total sea-levels, using Rahmstorf *et al.* [35] as a basis for sea-level rise projections. Estimates for Lunenburg, a neighboring community along the South Shore of Nova Scotia located northeast of the mouth of the LaHave estuary, are presented for 10, 25, 50 and 100-year return periods, for years 2000, 2025, 2055, 2085 and 2100.

For Lunenburg, this means that a 10-year storm could result in a sea-level of 3.29 m by 2025, 0.86 m higher than HHWLT (Higher High Water Large Tide). A 100-year storm in 2055 would increase water level to 3.80 m. The water levels in Table 1 are referenced to Chart Datum (CD), which is the same datum used for a hydrographic chart showing depths in the offshore and for tide tables. Note that CD typically represents the lowest possible tide in a local region, whereas topographic maps on land and lidar terrain models for this study are referenced to the Canadian Geodetic Vertical Datum of 1928 (CGVD28); water levels for this study have been converted from CD to CGVD28 using the offset of 1.01 m.

Table 1. Estimated extreme total sea levels (Higher High Water Large Tide (HHWLT) + Sea-Level Rise + Storm Surge) for return periods of 10, 25, 50 and 100 years for years 2000, 2025, 2050, 2085 and 2100. Lunenburg, HHWLT 2.43 m (Chart Datum), return period levels estimated as per Halifax tide gauge. From Richards and Daigle [45]. Error estimates are from [46] and represent 95% confidence intervals.

Extreme Total Sea Level [meters Chart Datum (CD)]—Lunenburg						
Return Period	**Residual**	**Level 2000**	**Level 2025**	**Level 2055**	**Level 2085**	**Level 2100**
10 Years	0.71 ± 0.20	3.14 ± 0.20	3.29 ± 0.23	3.57 ± 0.35	3.97 ± 0.56	4.20 ± 0.68
25 Years	0.81 ± 0.20	3.24 ± 0.20	3.39 ± 0.23	3.67 ± 0.35	4.07 ± 0.56	4.30 ± 0.68
50 Years	0.88 ± 0.20	3.31 ± 0.20	3.46 ± 0.23	3.73 ± 0.35	4.14 ± 0.56	4.37 ± 0.68
100 Years	0.95 ± 0.20	3.38 ± 0.20	3.53 ± 0.23	3.80 ± 0.35	4.21 ± 0.56	4.44 ± 0.68

1.4. Fluvial Flooding

Fluvial flooding is a common occurrence in the LaHave watershed. Fluvial flooding is caused when high or intense precipitation, or snow and ice melt within the watershed flows into the river, causing it to overtop its banks. High or intense precipitation is defined using Environment Canada's Rainfall Warning Criteria, wherein warnings are issued when 25 mm or more of rain is expected in one hour, when 50 mm or more is expected within 24 h or 75 mm or more within 48 h during the summer, or when 25 mm or more of rain is expected within 24 h during the winter [47]. While flooding from snow and ice melt can be predicted, flash flooding from sudden downpours can be more of a challenge to forecast [48].

The permeability of the land affects the ability of the land to absorb water and contributes to the severity of a fluvial flood. Frozen or saturated land could have temporary low permeability, while developed land or rocks such as shale and unfractured granite have permanently low permeability. Land cover such as pavement, ditched farmland, and deforested areas contribute to the amount of runoff entering a river, and can worsen the severity of fluvial flooding. For the LaHave River watershed, an analysis of satellite images to detect land use change indicated that approximately 75 km^2 of land was clearcut between 2004 and 2009, or about 4% of the area of the watershed. Land cover and deforestation

can also affect evapotranspiration, the total amount of moisture removed from the drainage basin by evaporation and plant transpiration.

Flow in the LaHave River follows a typical pattern, with maximum flow occurring in the spring and minimum flow occurring in the summer. An analysis of the 95-year LaHave River flow time series derived from the Environment Canada water level gauge in West Northfield (Figure 1) shows that almost 80% of the floods during that time period occurred during winter or spring, times when snow melt is likely to have contributed to the flood [49]. Maximum Instantaneous Peak Flow was highest on 10 January 1956 (1080 m^3/s) and second-highest on March 31, 2003 (663 m^3/s). Both of these floods were caused by heavy rain and melting snow and caused the highest water levels ever recorded (5.73 m and 5.17 m for 1956 and 2003, respectively), 1.5 to 2.0 m higher than any other flood event in the LaHave River watershed ([49]). Two fatalities occurred upstream of Bridgewater in 2003 when a car was swept into the flooded river [50].

1.5. Precipitation and Climate Change

As is the case with temperature and sea-level, precipitation and river discharge patterns are changing with climate change. In studies of precipitation in Atlantic Canada during the last half of the 20th century, Bruce *et al.* [51] report an increasing trend in the number of daily precipitation events >20 mm, and Mekis and Hogg [52] note an increase in the fraction of total precipitation falling in heavy events.

There are many different scenarios for how precipitation patterns will change with climate change, although there does seem to be consensus that there will be much more variability in the amount and frequency of intense rainfall in Nova Scotia [45,51,53] and in the Northeastern United States [54–56]. Richards and Daigle [45] project a variety of climate variables into the future based on an ensemble of several climate models. For Bridgewater, they predict an annual increase in precipitation; most of that increase is predicted to occur in the winter and spring, with minimal increase in summer and fall precipitation. Extreme rainfalls that happened only once every 50 years in the last century could occur once every 10 years in this century [57], and precipitation is expected to vary more from season to season and from year to year. Natural Resources Canada (NRCan) [53] predicts that Atlantic Canada will have hotter and drier summers, warmer winters, and more precipitation to fall as rain rather than snow. Conversely, Bruce *et al.* [51] predict a slight decrease in precipitation in the southern Maritime Provinces.

A study on global warming and precipitation in the United States reports that snowstorms and rainstorms have already become 30% more frequent and more severe than in 1948, producing 10% more precipitation, on average [54]. Of particular note to Atlantic Canada is the reported 85% increase in frequency of extreme rainfall and snowfall events in New England, meaning that a storm that used to occur every 12 months now occurs on average every 6.5 months. Singh *et al* [55] also predict an increase in precipitation amounts and frequency in coastal areas of the Northeastern United States, and Toreti *et al.* [56] use high resolution global climate models to predict a significant intensification of daily precipitation extremes for all seasons.

Studies of streamflow patterns during the last 50 years show that maritime rivers in the Atlantic provinces have been experiencing lower summer flows, but higher flows in early winter and spring [58,59]. Streamflow is expected to increase with temperature and precipitation in the Atlantic region [60], and

spring flood could become more common due to changes in late-winter early-spring precipitation patterns [61].

2. Methods

2.1. Hydrology Data

The factors driving the potential for flood risk in the Town of Bridgewater include weather, river stage and tides; these data are required to run the hydrological model and predict flood risk. Environment Canada monitors the water level or stage of the LaHave River and through the use of a rating curve and publishes discharge for the river [49], (Figure 1B). We have used these discharge data as the main input to the one dimensional river runoff model. Two water level sensors (tide gauges) were deployed by AGRG: one at the Marine Terminal within the Town of Bridgewater to measure water level in the town (Figure 1C) and one at Kraut Point to measure the water level near the mouth of the river (Figure 1D). Two AGRG weather stations were deployed: one at Cherryfield in the center of the watershed (Figure 1A) and another at Hirtles Beach along the Atlantic coast (Figure 1E). The station at Hirtles Beach was used to monitor the coastal conditions, and the measured barometric pressure was used to compensate the Kraut Point tide gauge. A barometric pressure sensor was deployed at the Marine terminal and used to compensate the tide gauge located there.

2.2. DEM Development

An accurate representation of bathymetry and topography is essential for successful hydrodynamic flood risk modeling. In this study bathymetry data from a combination of data sources were combined with topographic lidar data to generate a continuous DEM that was used in the model.

2.2.1. Bathymetric Survey

A bathymetric grid was compiled from a variety of sources to accurately represent seabed and river channel bathymetry and geometry. Depth soundings from nautical charts produced by the Canadian Hydrographic Service (CHS) were used for offshore and tidal areas. The digital Chart 4381 information at a scale of 1:38,900 covered the offshore and the mouth of the LaHave River to approximately Kraut Point. These data were supplemented by digitizing additional soundings from the paper chart at a scale of 1:38,900 which extended from Kraut Point to Upper LaHave (Figure 2). Additional depth soundings were collected using a 15 foot aluminum boat and depth sounder for the section of the river from Upper LaHave to the northern town limits where the river becomes too shallow to safely navigate a boat (Figure 2a). For the areas upstream of Bridgewater a combination of depths were measured using the depth sounder mounted on a canoe and for extremely shallow locations RTK GPS and depth measurements were obtained manually by walking across the river (Figure 2b).

Figure 2. Topobathymetric data sets amalgamated in this study include high precision airborne lidar, Canadian Hydrographic Service (CHS) bathymetric charts, and bathymetric data collected by boat using depth sounder (**a**) and survey grade Real Time Kinematic (RTK) GPS (**b**). The extent of this figure is shown on Figure 1 as Area 1.

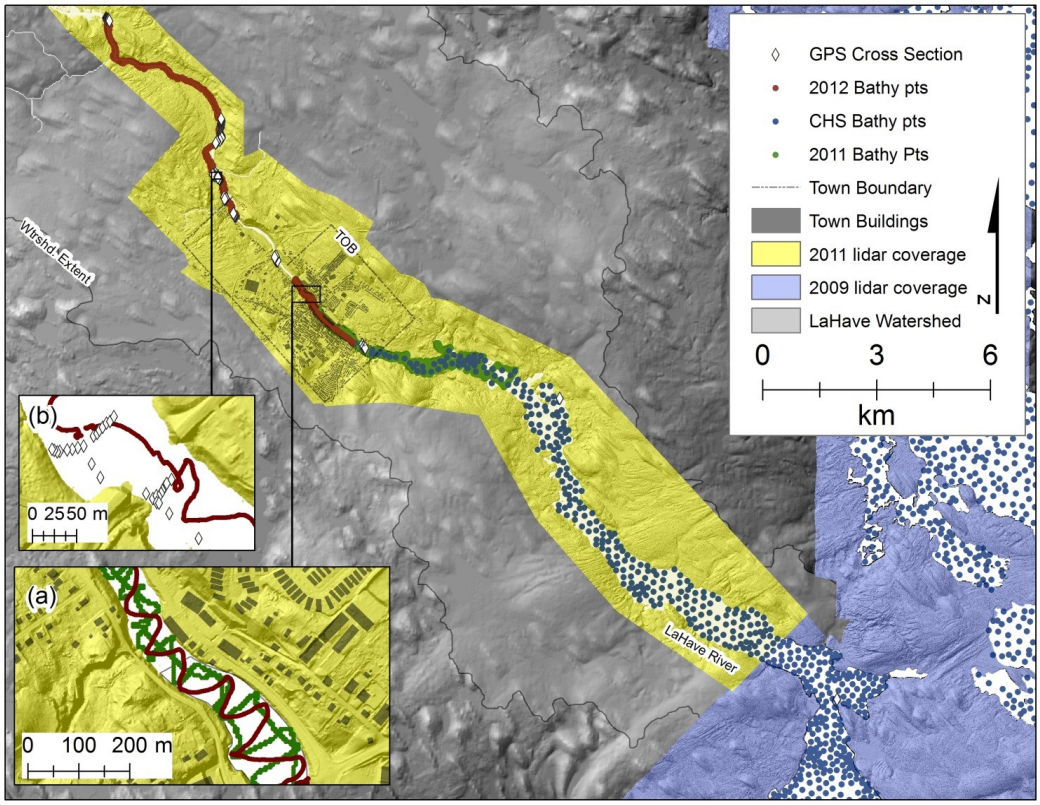

2.2.2. Lidar Survey

The coastline of Lunenburg County was surveyed with lidar in 2009 as part of the Atlantic Climate Adaptation Solutions (ACAS) project [1]. In order to conduct a flood risk study for the Town of Bridgewater a lidar survey was conducted in 11 and 12May 2012 by Leading Edge Geomatics (LEG) under contract to AGRG. The lidar survey area was from New Germany to East LaHave where it overlaps the coastal lidar acquired in 2009 (Figure 2). The lidar was collected with a ground point spacing of ~1 m and covers the major floodplain of the LaHave River and the entire Town of Bridgewater. LEG performed their own internal quality assurance on the data by comparing 26 point locations obtained with survey grade GPS to the lidar and reported a vertical Root Mean Square Error of 5 cm and a 9 cm error at the 95% confidence interval. The lidar point data were classified as "ground" and "non-ground" by LEG and delivered to AGRG. Two surface models were constructed from these data; a Digital Surface Model (DSM) which incorporates all the points and a bare-earth DEM which incorporates only the classified ground points. The lidar vertical accuracy was independently validated by AGRG who also collected survey grade GPS measurements to test the accuracy of the lidar. GPS points were collected along the roadway for the length of the survey. The GPS points were compared with the lidar DEM and the difference in elevation was calculated. The

mean difference between the DEM and GPS points was −0.05 m with a standard deviation of 0.06 m, which is consistent with the results of LEG.

2.2.3. Lidar—Bathymetry Integration

The LiDAR survey provides sufficient detail to model the floodplain but it does not penetrate the water surface, and must be combined with the bathymetry data to generate a seamless topo-bathymetric DEM that represents the topography above and below the water line. To achieve this, the river surface was delineated and removed from the terrestrial lidar dataset by sampling river elevations from cross sections along the length of the river, and intersecting the elevation model with the linear interpolation of the series cross sections per their minimum elevation plus 20 cm (Figure 3a). The resultant water surface polygon was then buffered by 5 m to classify river bank locations which were then amalgamated with all river bathymetric point data (Section 2.1) into a single point cloud of water depth, where river bank points (inside the 5 m buffer) were attributed 0 m depth. The bathymetry point cloud was sampled into a 10 m cell raster using average depth (Figure 3b). The 10 m binned depth average data were then interpolated into a continuous 1 m bathymetric raster surface using the minimum curvature spline method (Figure 3c). The river depth raster was then subtracted from the previously delineated lidar water surface raster (with a low pass filter applied) to generate a seamless hybrid topo-bathymetic elevation model of the river channel and surrounding topography with all elevations referenced to CGVD28.

Figure 3. A section of the LaHave River lidar elevation model (**a**) showing the cross sections used to procedurally delineate the water surface; (**b**) integrated bathymetric data and river bank points sampled to a 10 m average depth grid, and; (**c**) the interpolated 1 m river depth raster surface. The extent of this figure is shown on Figure 1 as Area 2.

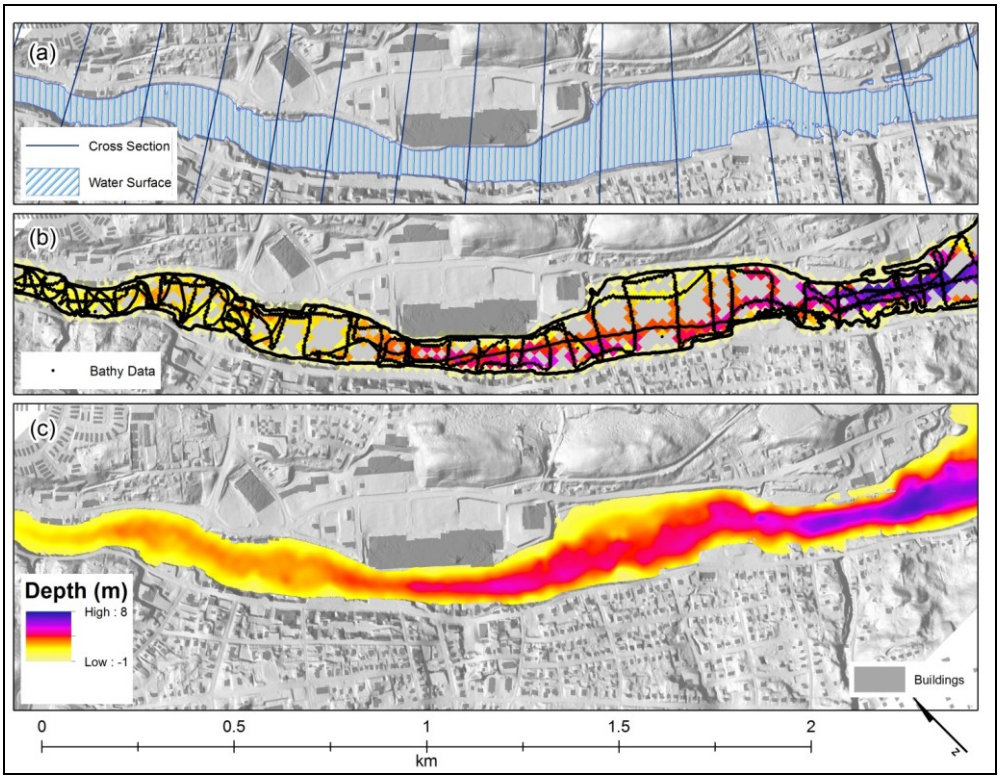

2.3. Hydrodynamic Modeling

Two types of models are used in this study, illustrated in Figure 4. The Mike-11™ model is used for river flooding and is a one dimensional (1-D) model that is based on cross-sections of the river and floodplain. The other type of model is a two dimensional (2-D) model known as Mike-21™, which is typically used for ocean and near shore circulation and tidal modeling. The two models are interfaced to produce a Mike Flood™ model which combines the discharge from Mike-11™ with the ocean levels from Mike-21™ and calculates the areas to be inundated based on the 2-D topography. The 1-D component of the model calculation performed based on the Saint Venant Equation which governs the conservation and continuity of momentum. Key assumptions of this approach include; a negligible variation in water density, a shallow river bottom slope, negligible vertical accelerations of water, and flow conditions remain subcritical. The 2-D component of the model simulates unsteady 2-D flows in one vertically homogenous fluid (depth averaged) and as such it assumes no large gradient of flow exists through the vertical water column. The governing equations conserve mass and momentum integrated over the vertical water column. The modelling system is based on the numerical solution of the two-dimensional impressionable Reynolds averaged Navier-Stokes equations subject to the assumptions of Boussinesq and of hydro-static pressure [62].

Figure 4. The model domain and boundaries of both the 1-D and 2-D components of the integrated coastal flooding simulation designed for the Town of Bridgewater (TOB). 1-D model components include: topo-bathymetric cross sections along river (in blue); 1A: the main channel discharge input; 1B, 1C, and 1D: discharge inputs for each major tributaries downstream; 1*: accumulated discharge inputs along the length of the 1-D domain (in a solid red line). 2-D model components include: three nested topo-bathymetric grids of 3 m, 9 m, and 27 m cell size; 6A: a tidal water level time series boundary; 5A, 5B: water level validation gauges deployed by AGRG.

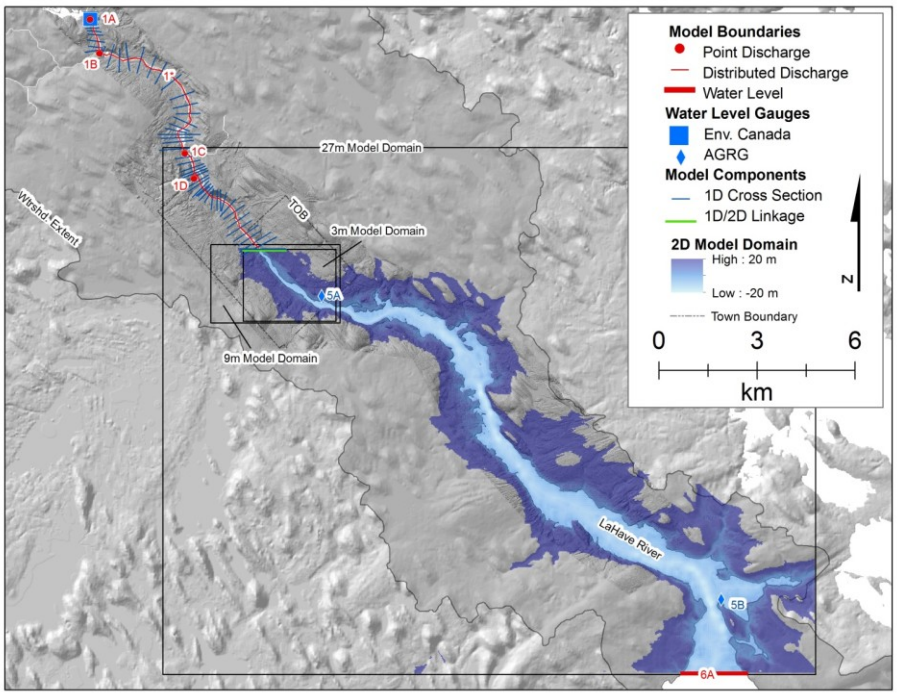

A nested grid approach was used allowing for concise transfer of mass and momentum across grid boundaries within the model domains, where the topography of the large area was represented by a 27 m grid which then was reduced by 1/3 to a 9 m grid around the Town of Bridgewater. This 9 m grid was further reduced by 1/3 to a 3 m grid to provide the most detail possible (Figure 4).

Downstream of the Environment Canada gauge (boundary 1A; Figure 4) there are several tributaries entering the main river channel (1B, 1C, and 1D; Figure 4). In order to account for their contribution to the hydrodynamic system, their respective discharges were estimated as proportional to the discharge rate determined for boundary 1A, based on their relative drainage areas. An accumulated discharge (1*; Figure 4) was also applied along the length of the 1-D portion of the main river channel relative to the discharge per drainage area of boundary 1A. The distributed drainage area was calculated as the total drainage area of the river at the end of the 1-D domain, minus the combined drainage areas of 1A, 1B, 1C, and 1D.

2.3.1. 1-D Model

A 1-D hydrodynamic model was developed using DHI's Mike-11™ for the LaHave River system from Bridgewater upstream to the Environment Canada water level gauge (Figure 4). In many studies of ungauged river systems, a watershed rainfall runoff model is developed to simulate the hydrological cycle within the area of study. This involves estimating parameters within the watershed that influence the amount of water that will infiltrate the ground *versus* runoff into the streams. In this study, however, since the LaHave River system has been gauged since 1915 and several major flooding events have been recorded, we have used the discharge record as a boundary condition for the Mike-11™ river model and thus no river-runoff model was necessary. The final simulations used the LaHave River discharge values to calculate the return periods of 50 and 100 year discharges under probabilities of 65% (at least one occurrence) and 99.5% (multiple occurrences) probability. The 65% probability analysis gives values for events that will occur at least once in 50 years (50 year return period) and at least once in 100 years (100 year return period), and are commonly used by planners who are interested in worst case scenarios. The 99.5% probability analysis gives values for events that could happen more frequently within the 50 and 100 year periods, and are more useful for Emergency Measures officials interested in these more frequent events (higher probability of occurrence) that will cause multiple floods. Once specific return period discharge values were calculated, hydrographs representing those discharge values were simulated and used as a boundary condition for the 1-D river runoff component of the model. The shape of the discharge curves used to simulate peak river runoff events was determined based on the signatures of observed extreme discharge from the LaHave River gauging station.

The most common method to determine the return periods of extreme events is to use statistical methods to determine the probability of occurrence or return period of certain events. In this study we are examining the risk of flooding from two possible sources which can interact to compound the problem; river runoff and storm surges or long-term sea-level rise. In order to calculate the risk of an extreme event occurring, a time series of events is used to examine how often such events have occurred in the past [39].

The time series of measured discharge of the LaHave River (Figure 5a) was used to determine the annual probability of extreme events and also the return period of extreme high flow events. Extreme Value Models (EVMs) are commonly used to determine the return periods of extreme events [46,63]. In order to capture the major floods of 1956 and 2003, several EVMs were fitted to the LaHave annual discharge maxima and compared to measured discharge values. The Gumbel distribution was chosen because the Gumbel EVM line fell between the two most extreme flow events of 1956 and 2003 and best represented the extreme values (Figure 5c).

Figure 5. (**a**) Time series of daily, annual mean and annual maximum discharge (m^3/s) of the LaHave River from the Environment Canada gauge. Red asterisks represent the flooding in 1956 and 2003; (**b**) Design Level graph for LaHave River discharge at 99.5% and 65% probability; (**c**) the Gumbel distribution used to model annual maximum LaHave discharge.

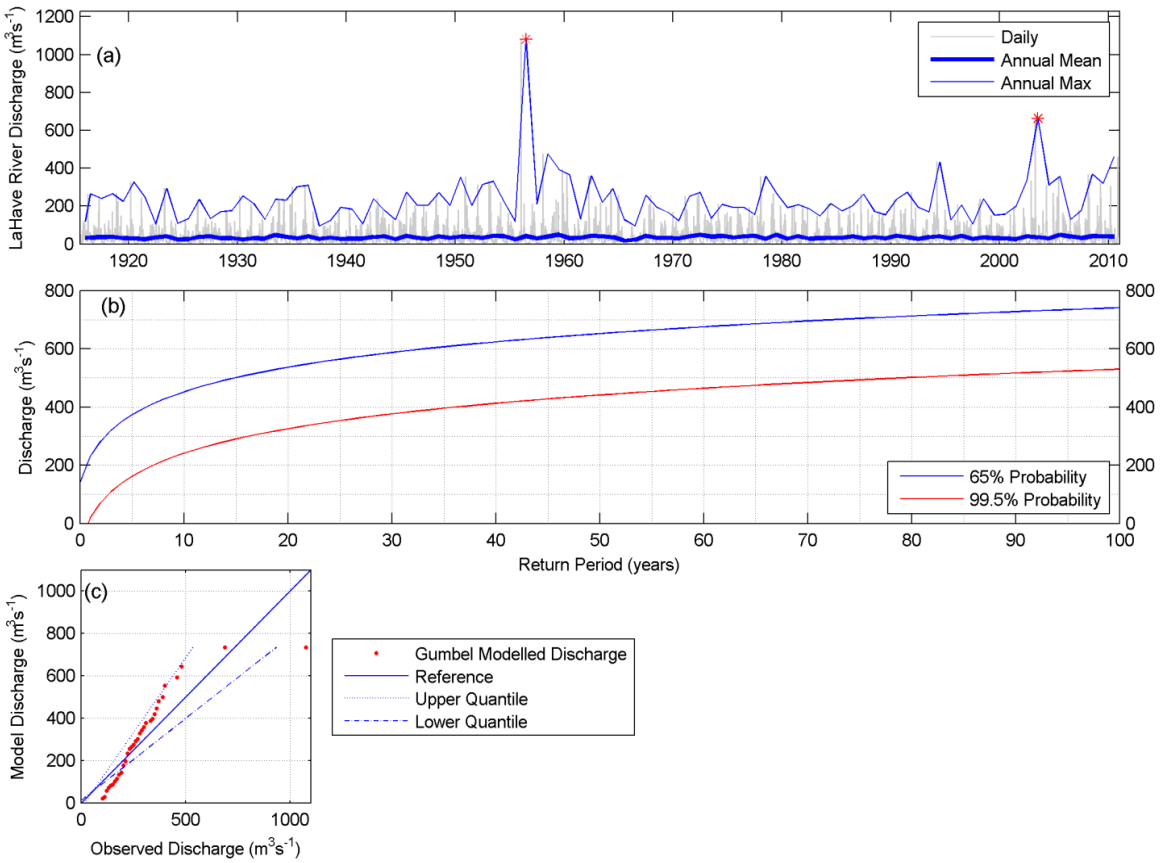

The EVM is used to set a fixed probability of an event occurring and then calculate the discharge value for different return periods. This is the method used to estimate the 50 and 100 year return periods of extreme discharge events (Figure 5b). This approach is also known as the Design Level where structures must be designed to withstand a certain level (water level, weight, *etc.*). If one chooses a probability of occurrence of 65% which equals at least one occurrence, then the Design Level can be calculated and the discharge for different return periods can be obtained. Thus for a 65% probability the 50 year discharge value is 652 m^3/s, whereas the 100 year return period corresponds to a 741 m^3/s discharge event (Figure 5b). Alternatively, one can examine the Design Level of a higher probability of 99.5% to calculate the discharge for the 50 and 100 year return period. With this higher

probability the 50 year return event has a discharge of 441 m^3/s and the 100 year event has a discharge of 530 m^3/s. With the higher probability of occurrence the discharge is lower for a given return period since it is expected to occur more frequently. Table 2 summarizes the discharge event probabilities, return period in years and the associated discharge. Re-examining the historical high discharge events of January 1956 and March 2003, we see that the 1956 event has a recurrence interval greater than 100 years, while the 2003 event is approximately equivalent to a 50 year return period event with a 65% probability of occurrence (Figure 5).

Table 2. Return periods with 65% and 99.5% probability of the 50 and 100 year discharge events.

Event Probability	Return Period in Years	Discharge (m^3/s)
65%	50	652
65%	100	741
99.5%	50	441
99.5%	100	530

2.3.2. 2-D Model

A high-resolution 2-D hydrodynamic model was developed using the DHI Mike-21™ software module to simulate tidal events. The bathymetry was represented by a grid which incorporated all of the depth sounding and coastal information (Figure 4). The bathymetry grid and domain of the model extended from the mouth of the LaHave River to upstream of Bridgewater, the maximum extent of tidal influence. This two dimensional hydrodynamic model provided the linkage between ocean tidal predictions and inland tidal events by simulating water level variations and flows over modeled bathymetry in response to a forcing tidal boundary condition at the southern extent of the LaHave River (Figure 4, 6A). The boundary condition was developed using the ocean tidal predictions obtained from a global tidal model supplied by DHI which was used to predict ocean elevation along the Atlantic Coast.

In order to estimate the risk or probability of flooding related to high water events along the coast, we used a similar method as described above for the river discharge to examine the Halifax tide gauge record back to 1919 from a previous study. Note that the tide measurements have been left relative to chart datum (CD), which for Halifax is 0.83 m below CGVD28. Mean sea-level has been rising in Halifax at a rate of 0.32 m/century and the annual maximum water level has been increasing at a rate of 0.34 m/century based on the best fit linear trend line of the tide gauge records (Figure 6a). Using the results from a previous study [1] where a Gumbel EVM was fitted to the distribution of the annual maximum water levels (Figure 6c) and a Design Level graph was generated for a probability of occurrence of 95% to determine what water levels are expected over time under different relative sea-level rise conditions (Figure 6b).

The 100 year water level under current Relative Sea-Level (RSL—global sea-level rise and crustal subsidence) rise conditions of 0.32 m/century is 3.03 m CD and increases to 3.32 m CD if RSL rises at a rate of 0.73 m/century [33] and further increases to 3.94 m CD if RSL rises at a rate of 1.46 m/century [35] (Figure 6b). Figure 6b shows that water levels as high as 2.4 m (CD) are expected to be seen within a return of 5 years regardless of the sea-level rise rate. The return period of water levels greater than 2.4 m (CD) are influenced by the sea-level rise rate. The predicted water levels rise quickly for all RSL

projections with return periods less than 10 years and begin to diverge and flatten out for longer return period events (Figure 6b).

Figure 6. (**a**) Halifax hourly, annual mean and annual maximum water levels above chart datum for 1920 to 2010, mean sea level rise (0.32 m/century) and maximum sea-level rise (0.34 m/century); (**b**) Design Level graph for Halifax. Expected water levels to be reached over time with different rates of relative sea-level (RSL) rise (m/century), green: current rate 0.32 m/century, blue: 0.73 m/century [33], red: 1.46 m/century [35]. Left vertical axis in CD, right vertical axis in CGVD28; (**c**) the Gumbel distribution used to model annual maximum sea level at Halifax.

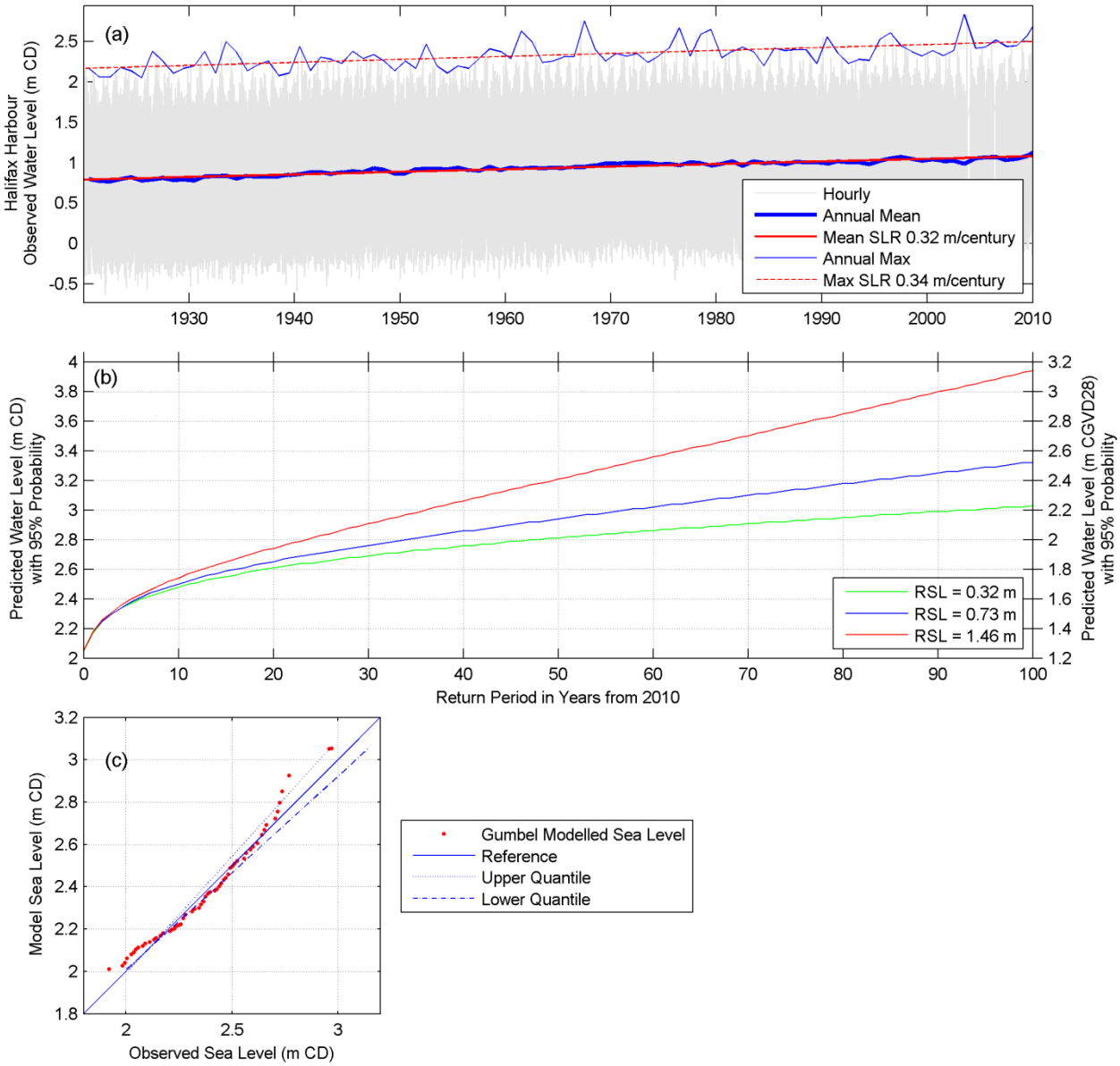

The 100 year return period water levels under different RSL conditions have been converted into the CGVD28 vertical datum for reference to the land DEM using a conversion of 0.83 m (Table 3). Figure 6b shows water levels referenced to CD on the left vertical axis and referenced to CGVD28 on the right vertical axis. The 100 year flood level under current RSL conditions is 2.2 m, which is 10 cm

below previous high water level maximum observed during Hurricane Juan in Halifax in 2003 which had an associated storm surge of 1.63 m [34]. If RSL increases to a rate of 0.73 m/century, the 100 year water level increases to 2.5 m CGVD28 which further inundates areas. If RSL increases to a rate of 1.46 m/century, the 100 year water level increases to 3.1 m CGVD28 which further inundates coastal areas.

Table 3. 100-year return period water levels for Halifax based on different sea-level rise scenarios.

Halifax Sea-Level Rise Scenarios (m/century)	100-year Return Period Water Levels (m CGVD28)
0.32	2.2
0.73 [33]	2.5
1.46 [35]	3.1

2.4. Model Simulations

Three sets of model simulations were executed for each different return period discharges: one set based on variable discharge under mean high tide conditions and two other sets based on different storm surge or long-term sea-level rise conditions (Table 4).

Table 4. Model simulations. The naming scheme of the simulations follows the format: the first 2–3 digits indicate a discharge return period of 50 or 100 years, the next 2 digits indicate the probability of occurrence being 65% or 99.5%, the last digits indicates the level of storm surge (0 for normal high tide conditions, 2 for a 2.2 m surge on top of the predicted tide or 3 for a 3.5 m surge on top of the predicted tide).

	LaHave River		Tidal Condition		
Probability	**Scenario**	**Discharge (m^3/s)**	**Mean High**	**Mean High + 2.2 m**	**Mean High + 3.5 m**
99.5%	50 year	441	50,990	50,992	50,993
	100 year	530	100,990	100,992	100,993
65%	50 year	652	50,650	50,652	50,653
	100 year	741	100,650	100,652	100,653

The period of the simulated storm surge signature was projected on top of the peak of the mean high predicted tide of the LaHave River mouth and was estimated from the relative period of observed storm surge residual of Hurricane Juan of 2003 from the nearby Halifax tide gauge. To model a storm surge event on the order of 2.2 m the value of 2.2 m was added to the predicted tide level. The selection of a 2.2 m storm surge was based partially on observations from the Halifax tide gauge where the storm surge for Hurricane Juan was measured at 1.63 m (it should be noted that this does not take into account waves). A larger value was selected in order to consider climate change and sea-level rise in the future. An additional set of simulations were executed with a 3.5 m storm surge at various river discharges in order to consider sea-level rise and the worst case scenario as outlined by Richards and Daigle [45]. The majority of the models were executed on the combined bathymetry and bare-earth lidar DEM. However, in order to evaluate the effect of buildings on the extent and movement of water we did construct one simulation using the building footprints and elevations imposed on the DEM. Flow velocities were affected, however the flood extents remained virtually the same, which for planning purposes was the focus of this study. There were several boundary conditions used for the

various simulations. The river discharge boundary condition was scaled proportionally to the drainage area for the LaHave River (Figure 7a) and the storm surge was added to the predicted mean high tide boundary at the mouth of the LaHave River (Figure 7b). The timing of the peak river discharge relative to the storm surge peak was determined experimentally, after calibrating for surface roughness, to ensure the worst case flooding condition downstream at the Town of Bridgewater.

Figure 7. (**a**) Black lines represent boundary conditions used for flood risk simulations for the LaHave River. Colored vertical scales represent how the boundary conditions scale with the drainage area (letters are shown in Figure 4); (**b**) tidal boundary conditions. The blue shading represents the start period and "warm up" of the model and the grey shading represents the time of the simulation and output.

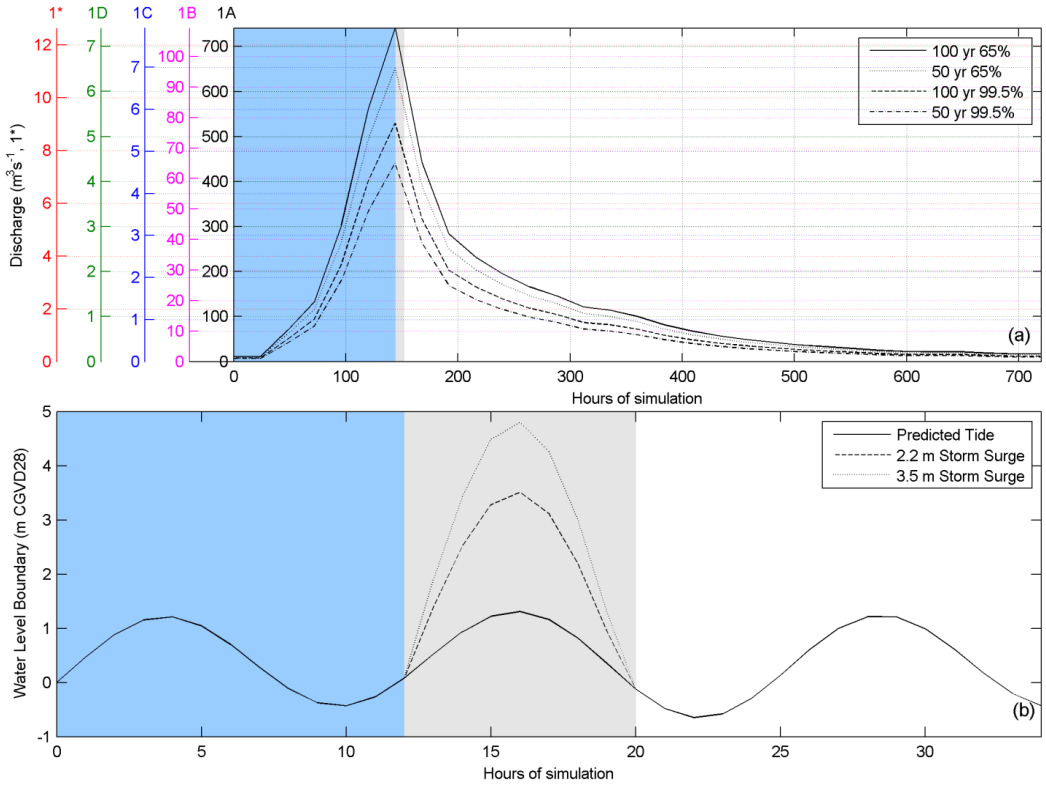

3. Results

3.1. Model Validation

The Mike-21™ hydrodynamic (HD) simulation was constructed and executed for validation purposes. Modeled water levels were compared with observations from the AGRG Marine Terminal tide gauge (Figures 4 and 5A) to evaluate model performance within the river. The channel between the wharf and land is relatively narrow where the tide gauge was located and not well represented on our model grid, even at 3 m; additionally, accurate bathymetry data for this area could not be obtained. As a result we extracted water levels from the model at a location close to the marine terminal in order to compare them to the observed water levels of the gauge. The Kraut Point tide gauge (Figures 4 and 5B) was used to evaluate the tidal dominant conditions for the Mike-21™ component of the model. River discharge was incorporated into the validation model using observed rates over the simulation time period.

In both cases where the tide gauge water level observations are compared to the model results, the model does not account for atmospheric forcing issues that could affect the observed water level such as wind. However, the validation results of the model indicate that over a four day period (October 23–27, 2012) the mean difference in observed and modeled water levels at Kraut Point (27 m grid domain) is −2.8 cm with a standard deviation of 7.1 cm (Figure 8a) and the mean difference in observed and modeled water levels at the Marine Terminal (3 m grid domain) is −3.8 cm with a standard deviation of 20.1 cm (Figure 8b). The increased noise in the water level observations at the Marine Terminal are interpreted to be a result of the finer grid cell size and the combined effects of river discharge and tide and the location of the gauge compared to the location where the model values were extracted. However, the results of the validation of the model are within the range of the absolute vertical accuracy of the lidar data (15–30 cm) and thus are considered suitable for lidar based flood mapping. The specific location chosen for the marine terminal tide gauge, being the shore side of the marine terminal wharf, may have further contributed to the apparent noise in both the gauged (green line) and modeled (blue line) water levels due to localized effects between the wharf and the shore and a lack of near shore bathymetry for that area (Figure 8b).

Figure 8. (**a**) Comparison of tide gauge observations with model results for the 27 m grid at Kraut Point (mean difference −2.8 cm, standard deviation 7.1 cm); (**b**) comparison of tide gauge observations with model results for the 3 m grid at the Marine Terminal (mean difference −3.8 cm, standard deviation 20.1 cm). Predicted tide used for the model boundary is plotted on both (**a**) and (**b**).

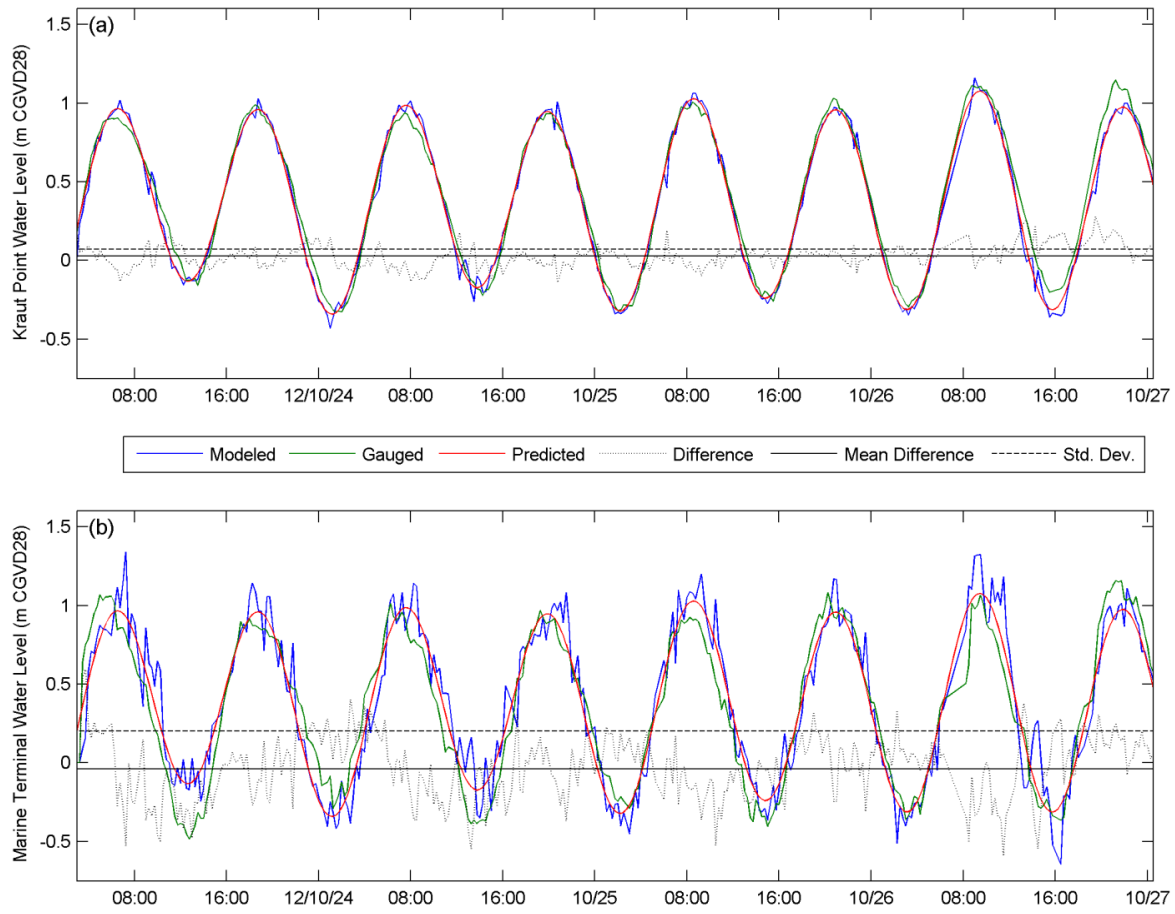

An assumed uniform bed roughness coefficient for both the 1-D and 2-D channels of a Manning's M = 32 (Manning's n = 0.0125) was applied, which corresponds to a clean, straight, full stage, open channel with some weeds and stones. This value was supported experimentally by the alignment of tidal signatures between the deployed gauges in the 2-D domain. The value was then assumed valid for the 1-D domain as no second river gauge was present to validate the rate of flow in this area; however, it was supported by field observations of the channel bottom. The homogenous surface roughness between two domains also facilitates a smooth boundary flow transition.

3.2. Model Simulation Results

The 1-D and 2-D modeled simulation results were draped on the DEM to build a flood risk map for each simulation described in Table 4. Each scenario was examined and compared to the other simulations to analyze the spatial extent of flooding.

Flood inundation from discharge alone under mean high tide conditions, a 50 year return period and at a 99.5% probability (sim50990) causes flooding upstream of the extent of tidal influence, which is just south of the Town Boundary (Figure 9a,d). The 50 year return period at a 65% probability, which is equal to at least 1 occurrence within 50 years, causes larger flood extents upstream of the Town Boundary due to the increased discharge (sim50650, not shown). Farther downstream the effects of flooding from 50 year return period discharge events (65% probability) at mean high tide are minimal (Figure 9b,c,e).

The 100 year return period of discharge at a 65% probability (sim100650), the highest discharge scenario, causes flooding upstream of the town to expand slightly (Figure 9). Adding a 2.2 m storm surge at the mouth of the LaHave River boundary (sim100652) causes sections of the town adjacent to the river to become inundated (Figure 9e). The parking lot surrounding the Bridgewater Mall floods (Figure 9b) the Marine Terminal Wharf is overtopped along with flooding of Shipyards Landing Park along the waterfront on the opposite side of the river from LaHave Street (Figure 9c). LaHave Street becomes inundated southeast of the Marine Terminal (Figure 9c).

The 100 year return period discharge at a 65% probability with a 3.5 m storm surge at the mouth of the LaHave River boundary (sim100653) results in even more sections of the town adjacent to the river becoming inundated (Figure 9b–d). The flood extends beyond the parking lot of the Bridgewater Mall and up to LaHave Street, and inundates additional commercial areas (Figure 9b). The flooding extends from overtopping the Marine Terminal Wharf to inundating LaHave Street on either side of the terminal (Figure 9c).

Areas upstream of the approximate range of tidal influence exhibit flooding only under discharge conditions but are not affected by the inclusion of storm surge (Figure 9a). Farther downstream (Figure 9d) an accumulation of floodwater occurs between discharge and storm surge water just upstream of the approximate normal tidal extent. Farther downstream still, (Figure 9e) low lying developments nearer the approximate normal tidal extent the of the river show no flooding during major discharge events alone (Figure 9e sim50990 and sim100650) but discharge is shown to increasingly exacerbate flooding when combined with storm surge floodwater for this area (*i.e.*, Figure 9e sim50992 and sim100652).

Figure 9. The various levels of flood risk for the Town of Bridgewater depicting outputs for combined 1-D and 2-D for; sim50990: 441 m^3/s discharge event with normal high tide; sim100650: 741 m^3/s discharge event with normal high tide; sim50992: 441 m^3/s discharge event with a 2.2 m storm surge amplification during a normal high tide; sim100652: 741 m^3/s discharge event with a 2.2 m storm surge amplification during a normal high tide; sim50653: 652 m^3/s discharge event with a 3.5 m storm surge amplification during a normal high tide; sim100653: 741 m^3/s discharge event with a 3.5 m storm surge amplification during a normal high tide (See Table 4).

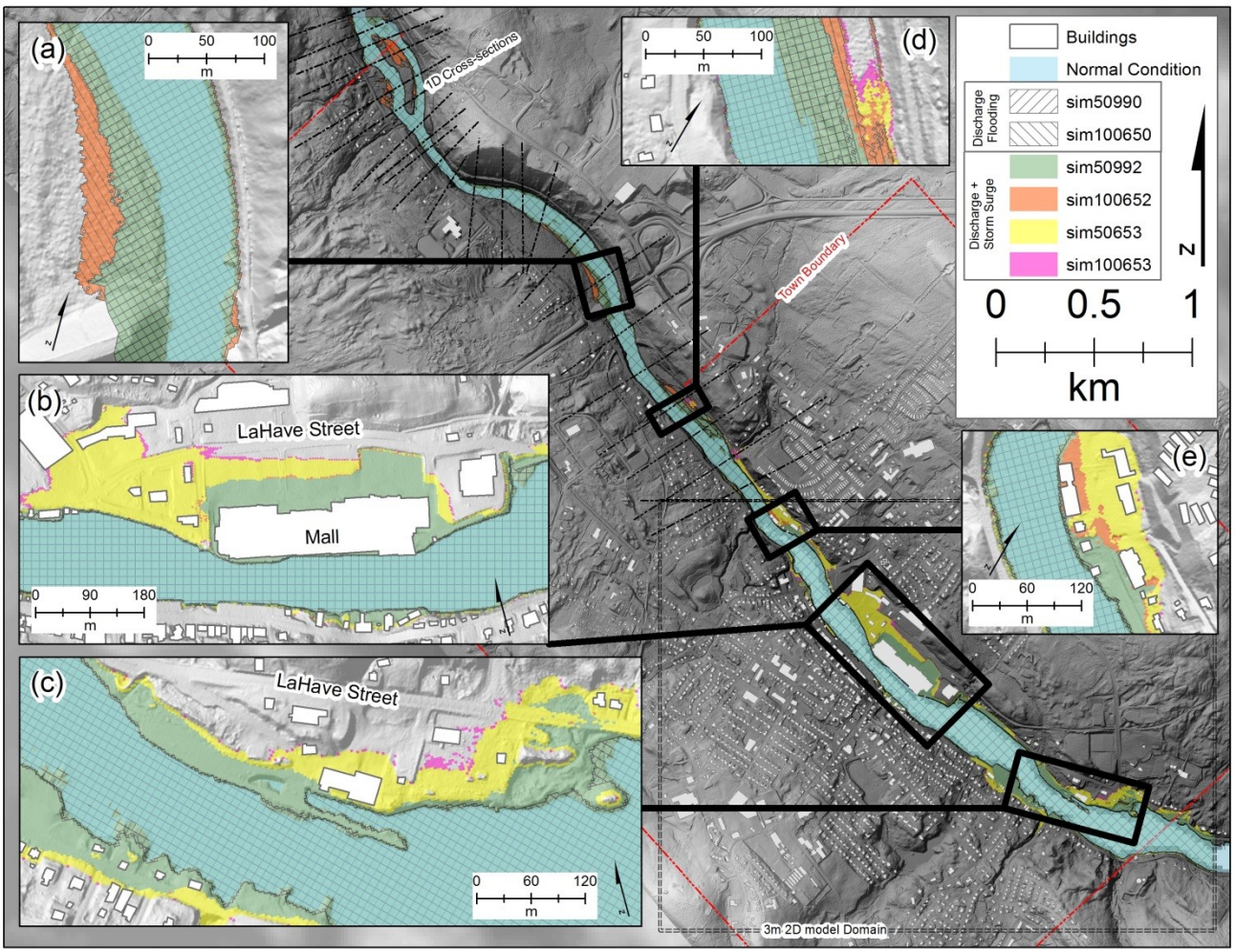

3.3. Discussion

3.3.1. Lidar-Bathymetry DEM

The high resolution lidar and the integration of bathymetry and river cross sections have enabled us to generate a hybrid DEM which was optimal for both fluvial and coastal flooding. Our findings are consistent with others [15–18] who indicate how using river bathymetry and cross-sections can improve model results for fluvial flooding. However, our results include three sources of bathymetry data that extends from the river flow gauge near the center of the watershed, out to and along the coast. This was necessary for our coupled discharge/storm surge model, but is a rarity in most flood risk studies.

The HD flood modeling was carried out using the bare-earth DEM from the lidar survey modified to include the bathymetry of the river channel. As a result, the flood extent does not include the buildings or other obstructions that are not represented in the DEM. Since capturing the complexities of urban topography is essential for providing good flood inundation maps [5–8], we assigned elevations to the building footprints and included them in the 3.5 m storm surge simulation. The results indicate that the inclusion of the buildings did not significantly change the flood extent or the time to drain the water back into the river. The buildings do have an effect on the water flow velocity that may result in increased erosion or other damage to the structures that was beyond the scope of this project. This maybe a result of the fact that a 3.5 m storm surge over a tidal cycle allows enough time for the water to inundate to a maximum level regardless of travel time. Even with a significant push upstream from a storm surge at the mouth of the river, the dominant flow direction downstream for the river is constant, although eddies appear in the current during the peak of the tide-surge with the river discharge. For visualization purposes, the flood inundation rasters from the seamless DEM simulations have been merged with an orthophoto and draped over the DSM in a perspective view. The extent of the flooding during mean high tide and with a 2.2 m and 3.5 m storm surge can be viewed in relation to familiar features, such as the shopping mall, and are easily explained to the public when the data are presented in this fashion (Figure 10).

3.3.2. Coupled 1-D/2-D Model

Using a coupled 1-D/2-D model was a preferred choice over either individual model type because it allowed us to more readily identify which regions were vulnerable to which types of floods. An analysis of the relative influence of tidal and river runoff components of flood risk along the LaHave River indicates that the main infrastructure of the town along the waterfront is more vulnerable to flooding as a result of storm surge events and long-term sea-level rise than river runoff events. However, the areas adjacent to the LaHave River upstream of the town are more influenced by runoff events than downstream, and are less affected by storm surge and sea-level rise. At the present time there is very little development and infrastructure in this upstream area. Flood risk mapping that accounts for the combined effect of sea-level rise and storm surge shows that the Bridgewater Mall, which was built on marshland, is especially vulnerable to flooding, along with several key transportation routes and parkland. In our study we confirmed the importance of elevated coastal water levels emphasized by [20,22] for increasing the risk of flooding for areas located inland from the coast. This type of coupled 1D-2D model is important for many communities that are located along estuaries and not directly on the coast. Many areas are already vulnerable to storm surges, and considering the expected sea-level rise associated with climate change, our methods and results can potentially be applied to areas that are not currently at risk but may be in the future. Additionally, our approach is easily modified for ever-changing estimates of sea-level rise.

Figure 10. A comparison of perspective views of the flood risk extents for various hydrodynamic models outputs. Each view is centered on the Bridgewater mall and looking down stream of the LaHave River with the 50 year return period discharge at 99.5% probability (441 m^3/sec). Simulated high water levels include; (**a**) Normal water level HD model, (**b**) Normal tide + 2.2 m storm surge HD model, and (**c**) Normal tide + 3.5 m storm surge HD model.

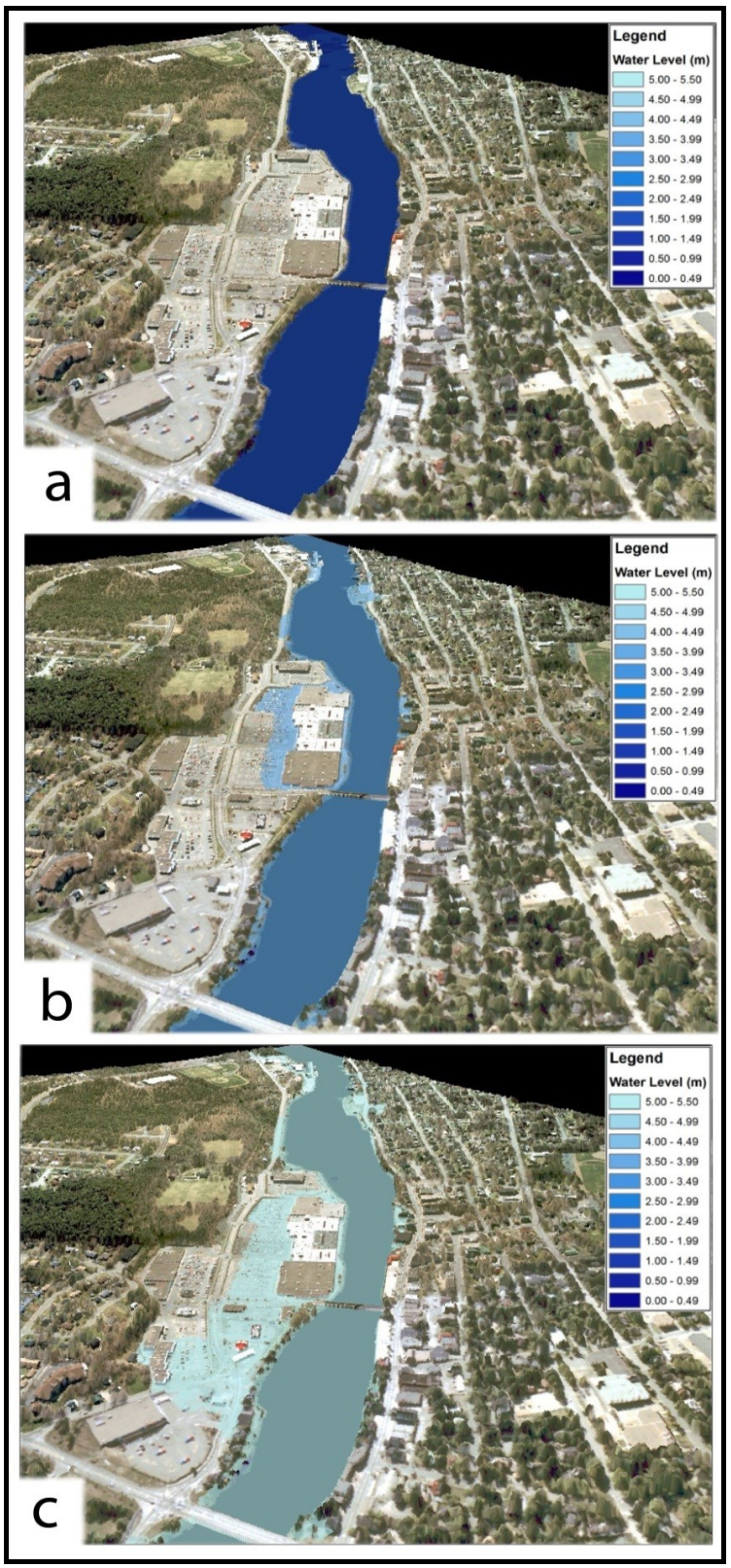

Drainage area is often used as a surrogate for discharge in many studies where watersheds are not gauged [64]. Few studies, however, examine the local hydrological effects of surface materials, such as glacial till cover, and groundwater interaction on discharge [65]. In our case the factors influencing the watershed hydrology were similar throughout the study area and thus allowed us to relate the drainage area directly to the discharge for given events. We further used this relationship to calculate the contributions of tributaries and the main channel downstream of the gauging station and upstream of our model boundary condition. The ability to utilize the relationship between discharge and drainage area provides confidence in our approach to supplement the discharge contribution of the downstream tributaries and main channel of the river based on the proportion of drainage area and discharge of the gauged section of the river.

3.3.3. Return Periods of Flow

As with sea-level rise, atmospheric climate projections contain much uncertainty. The projections by Richards and Daigle [44] extend only to 2080, and the authors express caution about the model's ability to predict extreme events. Although annual precipitation is expected to increase over time, the water surplus (runoff) is expected to decrease over time as a result of the increased temperature and thus increased evapotranspiration. The changes in short term precipitation (within a 24 h period) are expected to increase by 16% by 2080. These apparent contradictions in water surplus and short term precipitation are a reflection of the state of science with the ability of climate models to predict changes in extreme events rather than changes in mean climate indices. Given the uncertainty around this projection and its implications on flooding we have assumed the short term precipitation increase projection will translate into a 16% increase in discharge of the river. We have then used the extreme analysis method to calculate what effect this 16% increase in discharge will have on events. For example, a 16% increase in the flow of the 31 March 2003 flood event results in the return period from this event changing from a 53 year return period at 65% probability to a 44 year return event. In order to calculate how a 16% increase will affect the return period of the flows previously calculated for the present day we use the mean annual maximum flow of the LaHave River, so we are not looking at a single event but rather the average of the annual maximum runoff events. We then calculate what 16% of that flow is and use it as an average increase in river discharge by 2080. The current 50 year return period events drop by 3 years to a return period of 47 years in 2080 and the current 100 year return period events drop by 12 years to a return period of 88 years in 2080 (Table 5).

Table 5. Example of a 16% increase in short duration rainfall assumed to equal a 16% increase in the average annual maximum discharge. The current return period and discharge values for different probabilities and the return period projected to 2080 considering this 16% increase.

Event	Return Period in Years	Discharge (m^3/s)	Return Period (2080)
65% probability	50	652	47
65% probability	100	741	88
99.5% probability	50	441	47
99.5% probability	100	530	88

3.3.4. Maximum Flood Extent Mosaics

The result of the HD model for each time-step is a water elevation and water depth raster layer. There may be cases where a given time step does not produce the maximum flood extent for all areas on the map as a result of the dynamic nature of the model and the local topography gradient. This makes the output of the hydrodynamic model problematic to represent as a single GIS layer on a map. As a result, we have employed a new method that examined the outputs from the HD model and constructed a mosaic, which takes the maximum water level, or water depth, from the output time steps and constructs a raster mosaic of the maximum water elevation and water depth for each of the simulations. A shape file of the extent of the maximum flood extent from the mosaic has been determined and is provided for each simulation. While the model does account for hydro-connectivity in the 2-D domain, the isolated flooded cells visible in the output of sim100653 in Figure 9c are the result of binning model output by larger time steps (5 min) than the model run time (1 second). It is of note however, because the flood/dry depth was set quite low in our model, (0.002 m drying, 0.003 m flooding) these oscillations can represent very minor simulated flooding depths.

3.3.5. Study Limitations

The inundation model for the 3.5 m storm surge indicates that the floodwater extends beyond the mall parking lot and floods the area west of it. We have not modeled underground storm drainage systems however, and as such this inundation may not accurately reflect the proper drainage system. Though, if this area floods the elevation of the water in the river would be very high, thus prohibiting the drainage of this area through storm drains that empty into the river. In the case of the mall parking lot, after the storm surge water level subsides, the parking lot drains by surface runoff back into the river. This does not appear to be the case everywhere since there are areas where the water appears to get trapped in a low lying area with no means of overland flow back into the river.

Our model does, to a certain extent, account for bed roughness of the main channel as described in the model validation. However, the spatial variance of the bed roughness, especially upstream and in shallower waters was not extensively mapped and may have an effect on the rate of discharge in the upper stream. Future studies on the LaHave River will aim to include more upstream river gauges to observe for the rate of flow during high discharge events and can be used to empirically estimate bed roughness.

Furthermore, the combination of various environmental forcings has not been examined fully in this study. Principally, the combination of probabilities for river and coastal extreme events would naturally have a much larger accumulated return period, especially when the relative timing is taken into account. However the results of our study has indicated that the Town of Bridgewater is mainly susceptible to storm surge and thus further examination to the combined probabilities is less important than future analysis of storm surge and sea-level rise alone. Other complexities not considered in this study include atmospheric forcings such as the effect of ice build-up in the channel, snow melt in isolation of rainfall, and the increased flooding from wave run-up as the result of wind.

4. Conclusions

The methodology employed in this study can be applied to other estuarine locations where river runoff is potentially impeded by tidal water levels. The applicability of a model, such as Mike Flood, that can deal with river discharge and tidal interactions is required for such locations. A set of hydrodynamic flood simulations were conducted for the LaHave River for the town limits of Bridgewater. Past flooding events of the town and the LaHave River were researched and documented in this study. In order to conduct this work and support these modeling efforts, water level sensors were deployed at the Marine Terminal Wharf in the town and at Kraut Point near the mouth of the LaHave River. Field surveys were conducted to measure the topography of the river bed in order to merge this information with data acquired by a lidar survey of the study area. The bathymetry was merged with the lidar elevations to construct a seamless elevation model that was the basis for the flood risk model simulations. Environment Canada measures the stage of the LaHave River upstream of the town and converts these measurements into daily flow values. The time-series of flows dating back to 1913 were analyzed and the annual maximum flow was extracted. The annual maximum flow was used to fit an extreme value model to the data in order to calculate the return period of specific flood events, such as 31 March 2003. In addition the 50 year and 100 year flow levels were extracted from these data under different probabilities of occurrence. For example a 65% probability of occurrence is equivalent to at least once occurrence within the given return period. The river flows for the 50 and 100 year return periods were calculated for the 65% and 99.5% probability. The flows associated with these return periods were used to define the river discharge boundary at the upstream section of the river for the modeling. Since Bridgewater is located at the tidal extent of the LaHave Estuary, we also incorporated a tidal and storm surge component into the modeling. A tidal boundary was established near the mouth of the LaHave Estuary and the predicted tide was calibrated against the water level observations obtained from the water level sensor at Kraut Point. The tidal boundary used for the modeling consisted of a the mean annual high tide (1.5 m) as well as the simulation of a 2.2 m and 3.5 m storm surge event. This resulted in twelve simulations by combining the 50 and 100 year discharge events at 65% and 99.5% probability with normal high tide as well as normal high tide plus 2.2 m surge and normal high tide plus a 3.5 m surge. The selection of storm surge levels was made to account for future sea-level rise predictions under climate change.

Although there are a suite of uncertainties associated with this analysis that can be cumulative, including the accuracy of the input datasets, interpolation methods employed, hydrodynamics, model boundaries and timing of peak discharge and storm surge, our goal was to present planning officials and managers with easy to interpret map products of worst case possible outcomes of flood risk for the town. In order to keep the map output simple and easy to interpret, the uncertainties were not depicted on the map output. Accuracy assessments were presented for the input data and model validation to provide a level of confidence in the model and map output. In order to represent the uncertainties on the map, one would have to produce multiple flood polygons or apply some type of fuzzy boundary to the flood extent and thus make the map more difficult to interpret. The communication of uncertainty in such studies is challenging and is an active area of research. The results of the various flood risk simulations indicate that the area upstream of the approximate tidal extent is vulnerable to flooding from large discharge events of the LaHave River, while the downtown waterfront does not appear to be

susceptible to flooding from significant discharge events. This is probably a result of the deeper river channel in this area. However, the downtown area is vulnerable to SLR and storm surge flooding. The downtown nearest the river experience flooding under a 2.2 m storm surge generated at the mouth of the LaHave River, and much of the downtown infrastructure is inundated when the storm surge level is increased to 3.5 m. In some areas of the downtown the water appears to get trapped and does not easily drain back into the river once the storm surge levels subside. Although downtown Bridgewater is at risk only from extreme storm surge events, the risk will increase in the future with projected sea-level rise.

Acknowledgments

We thank Leon de Vreede and Eric Shaw, Bridgewater Planning Commission, for providing guidance and the funding for this study. Thanks also to Jeff Merrill, Acting Director of Planning for the District of the Municipality of Lunenburg and Bob Pett, Nova Scotia Department of Transportation and Infrastructure Renewal, for contributing to the lidar survey. We would like to thank from AGRG-NSCC Chris Webster, Charity Mouland, Nathan Parker, Wayne Reiger, and May Kongwonthai for various field and data processing assistance to the project and Brenda Veinot for assisting with the manuscript. We would like to thank the two anonymous reviewers for their comments which have improved this manuscript.

Conflicts of Interest

The authors declare no conflict of interest.

References

1. Webster, T.; McGuigan, K.; MacDonald, C. *LiDAR Processing and Flood Risk Mapping for Coastal Areas in the District of Lunenburg, Town and District of Yarmouth, Amherst, County Cumberland, Wolfville and Windsor*; Atlantic Climate Adaptation Solutions Association: Halifax, Canada, 2011; p. 130.
2. Webster, T.; Crowell, N.; McGuigan, K.; Collins, K. *Integrated River and Coastal Hydrodynamic Flood Risk Mapping*; Atlantic Climate Adaptation Solutions Association: Halifax, Canada, 2012; p. 43.
3. Webster, T.; McGuigan, K.; Crowell, N.; Collins, K. *River Flood Risk Study of the Nappan River Incorporating Climate Change*; Atlantic Climate Adaptation Solutions Association: Halifax, Canada, 2012; p. 48.
4. Webster, T.; Smith, T.; Collins, K. *Inventory of Physical Wastewater Infrastructure at Risk of Flooding to Climate Change induced Sea-level Incursions in the Minas Basin Area*; Atlantic Climate Adaptation Solutions Association: Halifax, Canada, 2012.
5. Haile, A.T.; Rientjes, T.H.M. Effects of Lidar DEM resolution in flood modelling: A model sensitivity study for the city of Tegucigalpa, Honduras. In Proceedings of ISPRS WG III/3, III/4, V/3 Workshop "Laser scanning 2005", Enschede, the Netherlands, 12–14, September, 2005; pp. 168–173.

6. Mason, D.C.; Horritt, M.S.; Hunter, N.M.; Bates, P.D. Use of fused airborne scanning laser altimetry and digital map data for urban flood modelling. *Hydrol. Process*. **2007**, *21*, 1436–1447.
7. Abdullah, A.F.; Vojinovic, Z.; Rahman, A.A. A Methodology for Processing Raw LiDAR Data to Support Urban Flood Modelling Framework: Case Study—Kuala Lumpur Malaysia. In *Developments in Multidimensional Spatial Data Models*; Rahman, A.A., Boguslawski, P., Gold, C., Said, M.N., Eds.; Springer: Berlin, Germany, 2013; pp. 49–68.
8. Abderrezzak, K.E.K.; Paquier, A.; Mignot, E. Modelling flash flood propagation in urban areas using a two-dimensional numerical model. *Nat. Hazards* **2009**, *50*, 433–460.
9. Webster, T.; Forbes, D.L. Using airborne LIDAR to map exposure of coastal areas in Maritime Canada to flooding from storm-surge events: A review of recent experience. In Proceedings of Canadian Coastal Conference, Dartmouth, Canada, 6–9 November 2005.
10. Poulter, B.; Halpin, P.N. Raster modelling of coastal flooding from sea-level rise. *Int. J. Geogr. Inf. Sci.* **2008**, *22*, 167–182.
11. Webster, T.L.; Forbes, D.L.; Dickie, S.; Shreenan, R. Using topographic lidar to map flood risk from storm-surge events for Charlottetown, Prince Edward Island, Canada. *Can. J. Remote Sens.* **2004**, *30*, 64–76.
12. Webster, T.L.; Forbes, D.L. Airborne Laser Altimetry for Predictive Modeling of Coastal Storm-Surge Flooding. In *Remote Sensing of Aquatic Coastal Ecosystem Processes*; Richardson, L.L., LeDrew, E.F., Eds.; Springer Netherlands: Dordrecht, the Netherlands, 2006; pp. 157–182.
13. Webster, T.L.; Forbes, D.L.; MacKinnon, E.; Roberts, D. Flood-risk mapping for storm-surge events and sea-level rise using lidar for southeast New Brunswick. *Can. J. Remote Sens*. **2006**, *32*, 194–211.
14. Smith, R.A.E.; Bates, P.D.; Hayes, C. Evaluation of a coastal flood inundation model using hard and soft data. *Environ. Model. Softw*. **2012**, *30*, 35–46.
15. Cin, C.D.; Moens, L.; Dierickx, P.; Bastin, G.; Zech, Y. An integrated approach for realtime floodmap forecasting on the Belgian Meuse River. *Nat. Hazards* **2005**, *36*, 237–256.
16. Moore, M.R. Development of a High-Resolution 1D/2D Coupled Flood Simulation of Charles City, Iowa. Master's Thesis, University of Iowa, 2011. Available online: http://ir.uiowa.edu/cgi/viewcontent.cgi?article=2417&context=etd (accessed on 12 March 2014).
17. Casas, A.; Benito, G.; Thorndycraft, V.R.; Rico, M. The topographic data source of digital terrain models as a key element in the accuracy of hydraulic flood modelling. *Earth Surf. Process. Landforms* **2006**, *31*, 444–456.
18. Cook, A.; Merwade, V. Effect of topographic data, geometric configuration and modeling approach on flood inundation mapping. *J. Hydrol.* **2009**, *377*, 131–142.
19. Horritt, M.S.; Bates, P.D. Evaluation of 1D and 2D numerical models for predicting river flood inundation. *J. Hydrol.* **2002**, *268*, 87–99.
20. Brown, J.D.; Spencer, T.; Moeller, I. Modeling storm surge flooding of an urban area with particular reference to modeling uncertainties: A case study of Canvey Island, United Kingdom: Modeling storm surge flooding of an urban area. *Water Resour. Res.* **2007**, *43*, 1–22.
21. Gouldby, B.; Sayers, P.; Mulet-Marti, J.; Hassan, M.A.A.M.; Benwell, D. A methodology for regional-scale flood risk assessment. *Proc. ICE Water Manag*. **2008**, *161*, 169–182.

22. Webster, T.; Sangster, C.; Kingston, D.; Christian, M. High-Resolution Elevation and Image Data within the Bay of Fundy Coastal Zone, Nova Scotia, Canada. In *GIS for Coastal Zone Management*; Smith, J., Darius Bartlett, E., Eds.; CRC Press: Boca Raton, FL, USA, 2004.
23. Gilles, D.; Young, N.; Schroeder, H.; Piotrowski, J.; Chang, Y.-J. Inundation mapping initiatives of the Iowa Flood Center: Statewide coverage and detailed urban flooding analysis. *Water* **2012**, *4*, 85–106.
24. Patro, S.; Chatterjee, C.; Mohanty, S.; Singh, R.; Raghuwanshi, N.S. Flood inundation modeling using Mike Flood and remote sensing data. *J. Indian Soc. Remote Sens*. **2009**, *37*, 107–118.
25. Sto. Domingo, N.D.; Paludan, B.; Madsen, H.; Hansen, F.; Mark, O. *Climate Change and Storm Surges: Assessing Impacts on Your Coastal City Through Mike Flood Modeling*; Danish Hydraulic Institute Group: Copenhagen, Denmark, 2010; p. 11.
26. Neily, P.D.; Quigley, E.; Benjamin, L.; Stewart, B.; Duke, T. *Ecological Land Classification for Nova Scotia Volume 1—Mapping Nova Scotia's Terrestrial Ecosystems*; Nova Scotia Department of Natural Resources Renewable Resources Branch: Halifax, Canada, 2003; p. 83.
27. Government of Canada; Environment Canada; Weather and Meteorology; Canadian Hurricane Centre—FAQ. Available online: http://www.ec.gc.ca/ouragans-hurricanes/default.asp?lang=En&n=3F0FD4CF-1#ws3C219DFF (accessed on 6 November 2013).
28. Taylor, R.B.; Frobel, D.; Forbes, D.L.; Mercer, D. *Impacts of Post-tropical Storm Noel (November, 2007) on the Atlantic Coastline of Nova Scotia*; Geological Survey of Canada: Dartmouth, Canada, 2008.
29. Hurricane Bill. Available online: http://past.theweathernetwork.com/your_weather/details/786/1442612/bridgewater/hits/1#utmxid=EAAAACD_N29-7CmDyYe4sM7ENrk;utmxpreview=0 (accessed on 12 March 2014).
30. IPCC. Summary for Policymakers. In *Climate Change 2013: The Physical Science Basis*; Contribution of Working Group I to the Fifth Assessment Report of the Intergovernmental Panel on Climate Change; Stocker, T.F., Qin, D., Plattner, G.-K., Tignor, M., Allen, S.K., Boschung, J., Nauels, A., Xia, Y., Bex, V., Midgley, P.M., Eds.; Cambridge University Press: Cambridge, UK, 2013.
31. Raper, S.C.B.; Braithwaite, R.J. Low sea level rise projections from mountain glaciers and icecaps under global warming. *Nature* **2006**, *439*, 311–313.
32. Church, J.A.; Gregory, J.M.; Huybrechts, P.; Kuhn, M.; Lambeck, K.; Nhuan, D.; Qin, D.; Woodworth, P.L. Changes in Sea Level. In *Climate Change 2001: The Scientific Basis*; Contribution of Working Group I to the Third Assessment Report of the Intergovernmental Panel; Douglas, B.C., Ramirez, A., Eds.; Cambridge University Press: Cambridge, UK, 2001.
33. Meehl, G.A.; Stocker, T.F.; Collins, W.D.; Friedlingstein, P.; Gaye, A.T.; Gregory, J.M.; Kitoh, A.; Knutti, R.; Murphy, J.M.; Noda, A.; *et al*. Global Climate Projections. In *Climate Change 2007: The Physical Science Basis*; Contribution of Working Group I to the Fourth Assessment Report of the Intergovernmental Panel on Climate Change; Solomon, S., Qin, D., Manning, M., Chen, Z., Marquis, M., Averyt, K.B., Tignor, M., Miller, H.L., Eds.; Cambridge University Press: Cambridge, UK, 2007.
34. Forbes, D.L.; Manson, G.K.; Charles, J.; Thompson, K.R.; Taylor, R.B. *Halifax Harbour Extreme Water Levels in the Context of Climate Change: Scenarios for a 100-Year Planning Horizon*; Natural Resources Canada: Ottawa, Canada, 2009; p. 22.

35. Rahmstorf, S.; Cazenave, A.; Church, J.A.; Hansen, J.E.; Keeling, R.F.; Parker, D.E.; Somerville, R.C.J. Recent climate observations compared to projections. *Science* **2007**, *316*, 709–709.
36. Shaw, J.; Taylor, R.B.; Forbes, D.L.; Ruz, M.-H.; Solomon, S. *Sensitivity of the Coasts of Canada to Sea-level Rise*; Natural Resources Canada: Ottawa, Canada, 1998; pp. 1–79.
37. Webster, T. Flood risk mapping using LiDAR for Annapolis Royal, Nova Scotia, Canada. *Open Access Remote Sens.* **2010**, *2*, 2060–2082.
38. Webster, T.; Stiff, D. The prediction and mapping of coastal flood risk associated with storm surge events and long-term sea level changes. In *Risk Analysis VI Simulations and Hazard Mitigation*; Brebbia, C.A., Beriatos, E., Eds.; WIT Press: Southampton, UK, 2008; pp. 129–139.
39. Webster, T.; Mosher, R.; Pearson, M. Water modeler: A component of a coastal zone decision support system to generate flood-risk maps from storm surge events and sea-level rise. *Geomatica* **2008**, *62*, 393–406.
40. Shaw, J.; Taylor, R.B.; Forbes, D.L.; Ruz, M.-H.; Solomon, S. *Sensitivity of the Canadian Coast to Sea-Level Rise*; Geological Survey of Canada: Otttawa, Canada, 1994; p. 114.
41. McCulloch, M.M.; Forbes, D.L.; Shaw, R.D. *Coastal Impacts of Climate Change and Sea-Level Rise on Prince Edward Island*; Geological Survey of Canada: Ottawa, Canada, 2002.
42. Peltier, W.R. Global glacial isotasy and the surface of the ice-age earth: The ICE-5G (VM2) model and GRACE. *Annu. Rev. Earth Planet. Sci.* **2004**, *32*, 111–149.
43. Knutson, T.R.; McBride, J.L.; Chan, J.; Emanuel, K.; Holland, G.; Landsea, C.; Held, I.; Kossin, J.P.; Srivastava, A.K.; Sugi, M. Tropical cyclones and climate change. *Nat. Geosci.* **2010**, *3*, 157–163.
44. Emanuel, K. Increasing destructiveness of tropical cyclones over the past 30 years. *Nature* **2005**, *436*, 686–688.
45. Richards, W.; Daigle, R. *Scenarios and Guidance for Adaptation to Climate Change and Sea Level Rise- NS and PEI Municipalities*; Atlantic Climate Adaptation Solutions Association: Halifax, Canada, 2011; p. 87.
46. Bernier, N.B. Annual and Seasonal Extreme Sea Levels in the Northwest Atlantic: Hind Casts over the Last 40 Years and Projections for the Next Century. Ph.D. Thesis, Dalhousie University, Halifax, NS, USA, December 2005.
47. Environment Canada; Public Alerting Criteria. Available online: http://www.ec.gc.ca/meteo-weather/default.asp?lang=En&n=D9553AB5-1#rainfall (accessed on 6 November 2013).
48. Environment Canada; Causes of Flooding. Available online: http://www.ec.gc.ca/eau-water/default.asp?lang=En&n=E7EF8E56-1#snowmelt (accessed on 8 November 2013).
49. Government of Canada; Environment Canada; Real-time Hydrometric Data. Available online: http://www.wateroffice.ec.gc.ca/index_e.html (accessed on 22 November 2013).
50. Brown, L. Flooded LaHave Claims Two Lives. *South Shore*, 9 April 2003.
51. Bruce, J.; Burton, I.; Martin, H.; Mills, B.; Mortsch, L. *Water Sector: Vulnerability and Adaptation to Climate Change*; Final Report; GCSI—Global Change Strategies International Inc. and The Meteorological Service of Canada: Ottawa, Canada, 2000.
52. Mekis, E.; Hogg, W.D. Rehabilitation and analysis of Canadian daily precipitation time series. *Atmosphere-Ocean* **1999**, *37*, 53–85.

53. Government of Canada, Natural Resources Canada. Canada in a Changing Climate: Atlantic Canada. Available online: http://www.nrcan.gc.ca/earth-sciences/climate-change/community-adaptation/830 (accessed on 6 November 2013).
54. Madsen, T.; Willcox, N. *When It Rains, It Pours Global Warming and the Increase in Extreme Precipitation from 1948 to 2011*; Environment America Research & Policy Center: Boston, MA, USA, 2012.
55. Singh, D.; Tsiang, M.; Rajaratnam, B.; Diffenbaugh, N.S. Precipitation extremes over the continental United States in a transient, high-resolution, ensemble climate model experiment. *J. Geophys. Res. Atmospheres* **2013**, *118*, 7063–7086.
56. Toreti, A.; Naveau, P.; Zampieri, M.; Schindler, A.; Scoccimarro, E.; Xoplaki, E.; Dijkstra, H.A.; Gualdi, S.; Luterbacher, J. Projections of global changes in precipitation extremes from Coupled Model Intercomparison Project Phase 5 models. *Geophys. Res. Lett*. **2013**, *40*, 4887–4892.
57. Nova Scotia Environment. *Toward a Greener Future: Nova Scotia's Climate Change Action Plan*; Nova Scotia Department of Environment: Halifax, Canada, 2009.
58. Whitfield, P.H.; Cannon, A.J. Recent variations in climate and hydrology in Canada. *Can. Water Resour. J*. **2000**, *25*, 19–65.
59. Zhang, X.; Harvey, K.D.; Hogg, W.D.; Yuzyk, T.R. Trends in Canadian streamflow. *Water Resour. Res*. **2001**, *37*, 987–998.
60. Najjar, R.G.; Walker, H.A.; Anderson, P.J.; Barron, E.J.; Bord, R.J.; Gibson, J.R.; Kennedy, V.S.; Knight, C.G.; Megonigal, J.P.; OConnor, R.E.; *et al*. The potential impacts of climate change on the mid-Atlantic coastal region. *Clim. Res*. **2000**, *14*, 219–233.
61. Intergovernmental Panel on Climate Change Working Group II. *The Regional Impacts of Climate Change: An Assessment of Vulnerability*; Cambridge University Press: Cambridge, UK, 1998.
62. Danish Hydraulic Institute. MIKE 21 Flow Model Hydrodynamic Model Scientific Documentation; Danish Hydraulic Institute: Horsholm, Denmark, 2012.
63. Thompson, K.R.; Bernier, N.B.; Chan, P. Extreme sea levels, coastal flooding and climate change with a focus on Atlantic Canada. *Nat. Hazards* **2009**, *51*, 139–150.
64. Snyder, N.P.; Whipple, K.X.; Tucker, G.E.; Merritts, D.J. Landscape response to tectonic forcing: Digital elevation model analysis of stream profiles in the Mendocino triple junction region, northern California. *Geol. Soc. Am. Bull.* **2000**, *112*, 1250–1263.
65. Tague, C.; Grant, G.E. A geological framework for interpreting the low-flow regimes of Cascade streams, Willamette River Basin, Oregon. *Water Resour. Res*. **2004**, *40*, W04303.